J. Fluid Mech. (1992), *vol.* 244, *pp.* 201–224

Liquid-metal flows near a magnetic neutral point

By R. G. KENNY

Department of Pure and Applied Physics, UMIST, PO Box 88, Manchester M60 1QD, UK

(Received 4 October 1991 and in revised form 27 April 1992)

A liquid-metal flow impinging upon a region of non-uniform d.c. magnetic field experiences a certain amount of braking owing to the effect of Lorentz forces acting on the metal. Practical electromagnetic flow control devices utilize this property to alter the flow rate at which a liquid metal emerges from a receptacle. As a preliminary step to understanding the three-dimensional behaviour a numerical model is constructed which examines the two-dimensional flow of liquid metal passing through a quadrupole magnetic field generated by four line currents. In the vicinity of the local neutral point it is found that the nonlinear flow becomes unidirectional and linear. This linear behaviour agrees well with analytic solutions for flow through an infinitely extended neutral point. The generalized forms of the magnetic fields which permit unidirectional flows to exist are investigated in both axisymmetric and two-dimensional geometries. Examples of these fields include both the extended neutral point and the uniform transverse magnetic field present in Hartmann flow. The optimum conditions for braking the flow with a specified field are characterized by the pressure and volume data. These variables are derived from the model for a range of values of field strengths and Reynolds numbers and allow a comparison to be made with the asymptotic results obtained from the linear theory for two-dimensional flows. The numerical scheme may be adapted for any type of magnetic field and also permits extensions to the more realistic axisymmetric case.

1. Introduction

Magnetohydrodynamics (MHD) has assumed growing importance in the metallurgically based industries with its especial application to the control of liquid-metal flows. Electromagnetic (e.m.) flow control devices possess many advantages, of which the principal is their ability to penetrate solid shells and interact with the liquid metal held within. The absence of any direct physical contact between the e.m. device and the liquid metal has the added advantage of not introducing any impurities into the metal and avoiding corrosion of the device. These principles are employed, for example, in the operation of induction furnaces in which circulating fluid motions are induced in molten metal by the interaction between eddy currents in the metal and an applied a.c. magnetic field. This type of electromagnetic stirring prior to solidification can radically improve the quality of metal which is produced.

Another important application of e.m. flow control occurs in the regulation of the rate at which liquid metal falls from a tun dish. The means of controlling the flow through the exit nozzle is provided by an e.m. valve, which is a current-carrying coil encircling the exit nozzle. Regulation of the rate of fall of liquid metal is achieved by varying the high-frequency currents in the coil which in turn alters the magnetic field responsible for braking the flow. Working industrial models of this type are described in Garnier (1982) and Lillicrap (1989). Valves of this nature can be automated and

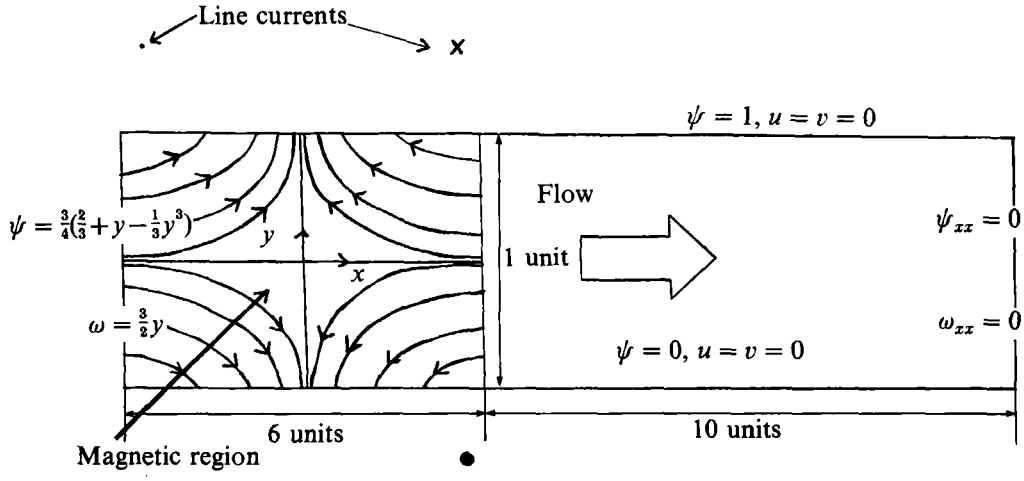

FIGURE 1. MHD duct flow in a non-uniform magnetic field generated by a quadrupolar arrangement of line currents.

incorporated into continuous manufacturing processes to provide regulated amounts of liquid metal from a tun dish into a series of receptacles passing below on a conveyor belt.

Many of the MHD applications in industry use high-frequency magnetic fields which are derived from a.c. current-carrying coils supplied by high-frequency power packs. In these cases the eddy currents induced on the surface of the particular liquid metal are much greater than the corresponding currents produced by the interaction between an equivalent d.c. field and the metal velocity. D.C. magnetic fields act throughout the liquid metal flow and need to be very large to produce currents comparable to the a.c. ones. Despite the less efficient action of d.c. fields they do find application as e.m. brakes, for example, in the continuous slab casting processes developed by ASEA (pointed out in a personal communication by H. Tinoco, 1987). In general, d.c. magnetic fields are cheap and safe to generate and perhaps with future improvements in technology (e.g. superconductors) they may produce effects on liquid-metal flows far surpassing those of comparable a.c. devices. Consequently, as the applications of d.c. magnetic fields become more extensive, better models of flow behaviour in various magnetic fields need to be established to enable prediction of flow behaviour. Unexpected and counter-intuitive results on the flows of liquid metals in magnetic fields have been observed and to a large extent modelled, but wide gaps remain to be bridged between experiment and theory, especially regarding flows in non-uniform fields.

In this paper we focus on the behaviour of a liquid-metal flow passing through a non-uniform d.c. magnetic field. The practical arrangement consists of a d.c. coil surrounding a pipe in which a specified flow of liquid metal is braked by the Lorentz forces acting throughout the flow. On account of the complexity of modelling a fully three-dimensional pipe flow through a non-uniform field, we initially consider the simpler case of two-dimensional duct flow with the current coil replaced by a quadrupole arrangement of line currents, figure 1. We hope to establish the parameter ranges for which a large pressure drop is induced in a given flow so that the device acts as an efficient d.c. brake.

The role of turbulence in MHD channel flows is not directly considered in this paper owing to the difficulty of modelling the problem of a fully time-dependent flow.

This does not mean that the flows modelled in this paper are unphysical since the omission of a detailed description of fluid turbulence can be justified by the tendency of the magnetic field to inhibit its generation. This behaviour is due to the reluctance of the field lines to be disturbed by small-scale fluctuations. Consequently, magnetic forces acting on the flow throughout the field domain tend to laminarize an otherwise pre-existing turbulent flow. It is also doubtful whether turbulence may be present to any significant extent both upstream and downstream of the magnetic region in the flows considered. This can be explained from general hydrodynamic considerations owing to the use of fairly small values of the Reynolds numbers in the calculations. Therefore, for suitable parameter ranges the results obtained from a turbulent-free MHD channel flow model are likely to closely reflect those found in experiment.

The general equations governing MHD channel flow are developed in §2 where particular mention is made of the boundary conditions upon the flow. A unidirectional solution of these equations is then found in §3 for the simpler problem of linear MHD flow through an extended neutral point in both axisymmetric and two-dimensional flows. Despite the unrealistic nature of the extended neutral-point field in the analytic model the study does serve to elucidate the likely behaviour of a fully developed flow impinging upon a region of non-uniform magnetic field containing a local neutral point. Unidirectional solutions to the MHD equations were first discussed by Pai (1954) and Regirer (1960) in axisymmetric and two-dimensional geometries respectively. Only specific forms of the magnetic field permit the existence of these types of solutions (Regirer 1960; Kenny 1990 – two-dimensional and axisymmetry respectively) which include the familiar Hartmann flow (Hartmann 1937; Shercliff 1965) through a uniform transverse magnetic field. The linear theory of a two-dimensional liquid metal flow through an extended magnetic neutral point predicts that in the limit of large magnetic field strengths the flow develops a 'jet-like' structure centred on the axis of the channel (Regirer 1960; Kenny 1989, 1990). A similar analytical study of the axisymmetric case is carried out in §3.1 and shows that in this case the unidirectional flow develops a slug (uniform) profile at large imposed field strengths in contrast to the two-dimensional neutral-point flow, Pai (1954).

In order to understand the full two-dimensional MHD flow behaviour a numerical model is constructed in §4 based upon the solution of the stream function–vorticity equation. The computational algorithm employs a compact scheme which is accurate to fourth order in the grid spacing and was first developed by Dennis (1985). In this model a specified duct flow impinges upon a region of non-uniform magnetic field which acts for a specified length of channel and compares realistically with the experimental situation in which the magnetic field of the e.m. device decays rapidly with distance along the duct. The non-uniform magnetic field contains a local neutral point and is generated by a quadrupolar arrangement of line currents external to the duct. After passing through this region of non-uniform field the flow emerges into a field-free region of channel where it finally settles down to Poiseuille flow.

Complications frequently arise in numerical models when quantities are estimated near to the boundaries and in this particular case the downstream conditions are suitably modified to give optimum numerical efficiency. These modifications and the nature of the boundary conditions incorporated into the numerical model are discussed in §5. A survey of the results obtained from the model is provided in §6. The dependence of the volume flux/pressure drop (at fixed pressure drop/volume flux respectively) upon a range of mean field strengths is examined and comparison made with derived asymptotic results. The velocity and vorticity profiles obtained

near the local neutral point are observed to accord well with the corresponding analytical study of flow through an extended two-dimensional neutral point (§3). These provide clear evidence that the fully nonlinear flow becomes unidirectional in the vicinity of the neutral point.

2. Equations

A brief summary of the relevant equations used to describe steady laminar MHD flow in a channel is now presented. The current distribution in such a flow is described by Ohm's law for a moving medium:

$$\boldsymbol{j}' = \sigma(\boldsymbol{E}' + \boldsymbol{u}' \times \boldsymbol{B}'), \tag{2.1}$$

where $\boldsymbol{j}'$ is the current density, σ the conductivity of the liquid metal, $\boldsymbol{E}'$ the electric field, $\boldsymbol{u}'$ the velocity and $\boldsymbol{B}'$ the total magnetic field. The magnetic field has two components: an imposed field $\boldsymbol{B}_0'$ and an induced component $\boldsymbol{b}'$, so that

$$\boldsymbol{B}' = \boldsymbol{B}_0' + \boldsymbol{b}'. \tag{2.2}$$

The induced magnetic field $\boldsymbol{b}'$ is generated from the current density $\boldsymbol{j}'$ (in (2.1)) according to Ampère's law:

$$\boldsymbol{j}' = (1/\mu_0)\nabla \times \boldsymbol{b}', \tag{2.3}$$

where μ_0 is the permeability of the liquid metal (more normally μ_0 is the permeability of a vacuum) and where it is assumed that the imposed field $\boldsymbol{B}_0'$ is not generated from any current sources within the flow. The interaction between the current distribution and magnetic field produces a Lorentz force which acts on the fluid so that an extra body force term appears in the Navier–Stokes equation,

$$\rho(\boldsymbol{u}' \cdot \nabla)\boldsymbol{u}' = -\nabla p' + \boldsymbol{j}' \times \boldsymbol{B}' + \mu \nabla^2 \boldsymbol{u}', \tag{2.4}$$

where p' is the pressure, μ is the viscosity and ρ is the density. The fluid is also assumed to be incompressible so that

$$\nabla \cdot \boldsymbol{u}' = 0. \tag{2.5}$$

Finally, from Maxwell's equations it follows that for steady flows

$$\nabla \cdot \boldsymbol{j}' = 0 \quad \text{and} \quad \nabla \times \boldsymbol{E}' = 0. \tag{2.6}$$

In order to generalize the equations of motion to those of similar flows the variables are non-dimensionalized in the following way:

$$\boldsymbol{u}' = U_0 \boldsymbol{u}, \quad \boldsymbol{B}' = B_0 \boldsymbol{B}, \quad \boldsymbol{j}' = \sigma U_0 B_0 \boldsymbol{j}, \quad \boldsymbol{b}' = B_0 \boldsymbol{b}, \quad p' = \rho U_0^2 p, \tag{2.7}$$

where U_0 and B_0 are typical values of the velocity and magnetic field respectively. The resulting equations take the form

$$\nabla \times \boldsymbol{b} = R_m \boldsymbol{j}, \tag{2.8}$$

$$\frac{1}{N}(\boldsymbol{u} \cdot \nabla)\boldsymbol{u} = -\frac{1}{N}\nabla p + \boldsymbol{j} \times \boldsymbol{B} + \frac{1}{M^2}\nabla^2 \boldsymbol{u}, \tag{2.9}$$

with

$$\boldsymbol{j} = \boldsymbol{E} + \boldsymbol{u} \times \boldsymbol{B}. \tag{2.10}$$

The parameters occurring in (2.8) and (2.9) are the interaction parameter N, the Hartmann number M and the magnetic Reynolds number R_m which can be expressed as

$$N = \sigma B_0^2 a/(U_0 \rho), \quad M^2 = \sigma B_0^2 a^2/\mu, \quad R_m = a U_0 \sigma \mu_0, \tag{2.11}$$

where a is a typical lengthscale. The parameters M and N are further related to the Reynolds number R by the relation

$$R = M^2/N = \rho U_0 a/\mu. \tag{2.12}$$

In reality flows are often turbulent and cannot be represented by the steady Navier–Stokes equations. Turbulence will be permitted in the model only in so far as it can be represented by a constant 'eddy viscosity'. In this case μ represents the eddy rather than the molecular viscosity.

We are principally interested in laboratory applications of MHD for which it is generally found that $R_m \ll 1$. In this limit R_m provides a measure of the ratio of induced field to the average applied field B_0. To first order in R_m we can ignore the nonlinear interaction between the velocity and magnetic fields and set $\boldsymbol{B} \approx \boldsymbol{B}_0$. This means that the Lorentz force occurring in (2.4) simply results from the interaction of the velocity field and the imposed magnetic field.

The vorticity description of the flow is obtained by taking the curl of (2.9) and after rearranging the parameters according to (2.12) one finds

$$\frac{1}{R}\nabla^2\boldsymbol{\Omega} - (\boldsymbol{u}\cdot\nabla)\boldsymbol{\Omega} + (\boldsymbol{\Omega}\cdot\nabla)\boldsymbol{u} = -N\nabla\times(\boldsymbol{j}\times\boldsymbol{B}_0), \tag{2.13}$$

where R is defined in (2.12) and $\boldsymbol{\Omega} = \nabla\times\boldsymbol{u}$ is the vorticity vector. The term on the right-hand side of (2.13) represents the curl of the Lorentz force and it will be seen to play a crucial role in determining the behaviour of the flow for large M. The nonlinear terms in (2.13) usually prevent analytical progress. However, there do exist some flows, considered in §4, for which $(\boldsymbol{u}\cdot\nabla)\boldsymbol{\Omega}$ and $(\boldsymbol{\Omega}\cdot\nabla)\boldsymbol{u}$ both vanish. These flows are unidirectional and are only produced by certain magnetic fields, examples of which include a uniform transverse field, giving rise to the much-studied Hartmann flow, and the less well-known neutral-point flow in both two dimensions and axisymmetry. A more general discussion of magnetic fields that permit unidirectional flow solutions to exist is given in §3.

3. Unidirectional neutral-point flows

The full set of MHD equations derived in §2, (2.5)–(2.10), are nonlinear and prevent any sort of analytical progress being made on them. However, if certain simplifying assumptions are made then it should be possible to find solutions which will bear some resemblance to real flow behaviour. A comparison of results obtained for flow in the neighbourhood of a two-dimensional neutral point using both numerical and analytical approaches is presented in §4. The good agreement exhibited by these two separate investigations implies that the full nonlinear flow in the vicinity of a neutral point is accurately modelled by the linear equations examined in this section.

The simplified model examined here consists of liquid-metal duct flows encountering extended magnetic neutral points in both axisymmetric and two-dimensional geometries as in figure 1. The magnetic neutral points in the two types of geometry are respectively described by $\boldsymbol{B}_0 = (r, 0, -2z)$ in terms of cylindrical coordinates (r, θ, z) and $\boldsymbol{B}_0 = (-x, y, 0)$ in terms of Cartesian coordinates (x, y, z). The idealization of the model arises in the simplified description of the neutral point which is assumed to extend throughout space. Such magnetic fields give rise to flows which are unidirectional, depending solely on the transverse coordinate of the particular duct

concerned. The nonlinearities in the MHD equations disappear for these unidirectional flows, since the terms $(\boldsymbol{u}\cdot\nabla)\boldsymbol{\Omega}$ and $(\boldsymbol{\Omega}\cdot\nabla)\boldsymbol{u}$ both vanish in (2.13).

The other unidirectional type of flow to have been extensively studied is Hartmann flow, which occurs in a uniform transverse magnetic field. This forms but one of a family of unidirectional solutions describing flow through non-uniform magnetic fields which vary in the direction of the channel. Only certain functional forms of these magnetic fields permit unidirectional solutions to exist and include for example the axisymmetric neutral point first considered by Pai (1954). Regirer (1960) gave a generalized prescription for the forms of the magnetic fields in two dimensions and then solved a related problem of unidirectional flow through an extended neutral point. In this paper we specialize his analysis to channel flow through an extended neutral point, in §3.3, and compare with the corresponding numerical model presented in §4 which examines fully developed flow impinging upon a non-uniform field containing a local neutral point. In the next section we examine the types of magnetic field which permit the existence of unidirectional solutions in axisymmetry. A little surprisingly the axisymmetric problem is mathematically simpler to manipulate than the two-dimensional case and so it is considered first.

3.1. *General axisymmetric neutral-point flow*

A conducting fluid flows through a non-conducting cylindrical pipe of radius a under the influence of an applied pressure difference and through an imposed magnetic field $\boldsymbol{B}_0$. We show that only a magnetic stream function of the form $\chi(r,z) = z(A_0r^2+A_1)+g(r)$ permits unidirectional solutions of the flow to exist in axisymmetric geometry.

The symmetry of the problem enables the magnetic field to be expressed in terms of the following vector potential:

$$\boldsymbol{B} = \nabla\times\left(\frac{\chi(r,z)}{r}\hat{\boldsymbol{\theta}}\right) = \frac{1}{r}\nabla\chi\times\hat{\boldsymbol{\theta}}, \tag{3.1}$$

where $\hat{\boldsymbol{\theta}}$ is a vector in the azimuthal direction of the pipe. The velocity is assumed to be unidirectional and lies solely in the axial or z-direction and has a functional dependency on the radial coordinate r only, since $\nabla\cdot\boldsymbol{u} = 0$, so that

$$\boldsymbol{u} = (0,0,u(r)). \tag{3.2}$$

We may simplify the equations of steady state motion derived in §2 using (3.1) and (3.2). For example Ohm's law (2.10) becomes

$$\boldsymbol{j} = \boldsymbol{E} - \frac{u\chi_z}{r}\hat{\boldsymbol{\theta}}. \tag{3.3}$$

Clearly, since $\nabla\cdot\boldsymbol{j} = 0$ from (2.6) and $\nabla\cdot(\boldsymbol{u}\times\boldsymbol{B}) = 0$ by inspection of the term on the right-hand side of (3.3) then it follows that $\nabla\cdot\boldsymbol{E} = 0$. This result combined with the steady-state results of Maxwell's equations in (2.6) implies that $\boldsymbol{E}$ is at most a constant vector. Taking advantage of the geometry of the problem and applying suitable boundary conditions we can set $\boldsymbol{E} = 0$.

The Navier–Stokes equation (2.9) linearizes once $\boldsymbol{u}$ is specified according to (3.2) so that we obtain

$$0 = -\frac{1}{N}\nabla p + \boldsymbol{j}\times\boldsymbol{B} + \frac{1}{M^2}\nabla^2\boldsymbol{u}, \tag{3.4}$$

applying the relations in (2.11). Substitution of the forms of $\boldsymbol{j}$, $\boldsymbol{B}$ and $\boldsymbol{u}$ yields an expression for the pressure gradient which has both axial and transverse components:

$$\frac{1}{N}\nabla p = -\frac{u\chi_z}{r^2}\nabla\chi + \frac{1}{M^2}\nabla^2 u(r)\,\hat{\boldsymbol{z}}. \tag{3.5}$$

The curl of (3.5) eliminates the pressure gradient, giving the vorticity equation in the $\hat{\boldsymbol{\theta}}$-direction relating $\chi(r,z)$ and $u(r)$ in the following manner:

$$\frac{\partial(\chi, u\chi_z/r^2)}{\partial(r,z)} + \frac{1}{M^2}\frac{\mathrm{d}}{\mathrm{d}r}\nabla^2 u(r) = 0. \tag{3.6}$$

Equation (3.6) is similar to the stream function–vorticity equation derived in (2.13); however, the latter was obtained on the assumption that $R_\mathrm{m} = 0$. The definition of $\boldsymbol{B}$ in (3.1) includes a component of induced field according to (2.2) and so here the general case of $R_\mathrm{m} \neq 0$ is considered. Equation (3.6) must be solved in tandem with Ohm's law (3.3) in which we express $\boldsymbol{j}$ in terms of $\chi(r,z)$ and $\hat{\boldsymbol{\theta}}$ using Ampère's law (2.8) to give

$$\boldsymbol{j} = \frac{1}{R_\mathrm{m}}\nabla\times\boldsymbol{B} = -\frac{1}{R_\mathrm{m}}\left(\nabla^2\left(\frac{\chi}{r}\right) - \frac{\chi}{r^3}\right)\hat{\boldsymbol{\theta}}, \tag{3.7}$$

which on substitution into (3.3) with $\boldsymbol{E} = 0$ yields

$$R_\mathrm{m}\, u\chi_z = \chi_{rr} - \chi_r/r + \chi_{zz}. \tag{3.8}$$

Equation (3.6) is a third-order differential equation for $u(r)$ whose coefficients must be independent of z. We therefore require

$$\chi_z = f(r). \tag{3.9}$$

Consequently, $\chi(r,z)$ has the following general form:

$$\chi(r,z) = zf(r) + g(r), \tag{3.10}$$

which upon substitution into (3.8) yields the two defining equations for $f(r)$ and $g(r)$:

$$f''(r) - f'(r)/r = 0, \tag{3.11}$$

and

$$g''(r) - g'(r)/r = R_\mathrm{m}\, u(r) f(r). \tag{3.12}$$

Solving (3.11) for the general form of $f(r)$ yields

$$f(r) = A_0 r^2 + A_1, \tag{3.13}$$

where A_0 and A_1 are constants. The defining equation for $g(r)$ from (3.12) then becomes

$$g''(r) - g'(r)/r = R_\mathrm{m}\, u(r)\,(A_0 r^2 + A_1). \tag{3.14}$$

We identify $g(r)$ as the stream function of the magnetic field induced by the current distribution in the flow given by (3.3). Consequently, the total magnetic field $\boldsymbol{B}$ can be expressed as the sum of an imposed field $\boldsymbol{B}_0$ and an induced field $\boldsymbol{b}$ such that

$$\boldsymbol{B} = \boldsymbol{B}_0 + \boldsymbol{b} = (-(A_0 r + A_1/r), 0, 2A_0 z) + (0, 0, g'(r)/r), \tag{3.15}$$

where $\nabla\times\boldsymbol{B}_0 = 0$ and $\nabla\times\boldsymbol{b} = R_\mathrm{m}\boldsymbol{j}$ inside the duct. If the field $\boldsymbol{B}_0$ is everywhere finite inside the pipe including the line $r = 0$ then we must have $A_1 = 0$. However, in the case of hollow pipes with a solid cylindrical core the A_1 term might be important.

The general form for the stream function $\chi(r\,z)$ which permits unidirectional velocity profiles to exist is expressed as

$$\chi(r,z) = A_0 r^2 z + g(r). \tag{3.16}$$

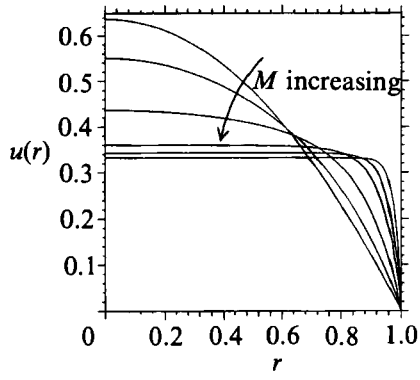

FIGURE 2. Axisymmetric velocity profiles at various values of the Hartmann number for unit flux.

3.2. *Axisymmetric neutral-point flow through a pipe*

It now becomes a matter of solving the vorticity equation expressed in (3.6) for the flow profile $u(r)$, assuming without loss of generality that $A_0 = -1$, to give

$$\boldsymbol{B} = \boldsymbol{B}_0 + \boldsymbol{b} = (r, 0, b(r) - 2z), \tag{3.17}$$

where $\boldsymbol{B}_0 = (r, 0, -2z)$, $\boldsymbol{b} = (0, 0, b(r))$ and $b(r) = g'(r)/r$. Upon substitution of (3.17) into (3.6) the following third-order differential equation for $u(r)$ is obtained:

$$u'''(r) + u''(r)/r - u'(1/r^2 + M^2 r^2) = 0, \tag{3.18}$$

where r is scaled so that $0 \leqslant r \leqslant 1$ and M is the Hartmann number defined in (2.11). In order to fully specify the flow three boundary conditions for $u(r)$ are required. Firstly, we impose the no-slip condition at the wall of the pipe, so that $u(1) = 0$, and secondly that the flow is symmetrical about the axis, giving $u'(0) = 0$. Finally, the impetus for the flow can be provided either by a fixed pressure gradient term in (3.4) or by a specified flow rate. The latter condition is employed in this case for ease of comparison with other flows and is set to unity. Equation (3.18) can be transformed to a second-order differential equation whose solution was originally derived by Pai (1954) and exhibits the form

$$u(r) = a_0(M) \int_{M^{\frac{1}{2}}r}^{M^{\frac{1}{2}}} \frac{\sin(\frac{1}{2}\xi^2)}{\xi} \mathrm{d}\xi, \tag{3.19}$$

where $a_0(M)$ is a constant determined by the volume flux and is given by

$$a_0(M) = (M/\pi)[\cosh(\tfrac{1}{2}M) - 1]^{-1}. \tag{3.20}$$

Figure 2 depicts the corresponding profiles for $u(r)$ at various values of the Hartmann number for unit flux. The induced magnetic field $\boldsymbol{b}$ can be deduced from Ohm's law (3.3) and (3.20) and behaves in the following manner:

$$b(r) = \frac{a_0(M) R_{\mathrm{m}}}{2M} \left[\cosh(\tfrac{1}{2}M) - \cosh(\tfrac{1}{2}Mr^2) - Mr^2 \int_{M^{\frac{1}{2}}r}^{M^{\frac{1}{2}}} \frac{\sinh(\frac{1}{2}\zeta^2)}{\zeta} \mathrm{d}\zeta \right], \tag{3.21}$$

using the boundary condition that $b(1) = 0$. Since there are no currents external to the pipe then $\nabla \times \boldsymbol{b} = 0$ there and the field vanishes outside, so that

$$b(r) = 0, \quad r \geqslant 1, \tag{3.22}$$

and matching at the wall gives $b(1) = 0$. Integrating the expression for the pressure gradient in (3.5) using (3.17) and (3.21) gives the pressure distribution,

$$p(r,z) = -kz - \frac{N}{2R_m} b^2(r) + \frac{2N}{R_m} b(r) z, \tag{3.23}$$

where k can be determined from (3.5) and (3.19). At large $\pm z$ the pressure still depends on r in contrast to Poiseuille flow in which no cross-channel pressure gradients exist. This behaviour is a consequence of the infinite extent of action of the magnetic field.

The tapering form of the applied magnetic field in (3.17) might lead one to expect a concentration of flow towards the axis of the channel for large values of M. The Lorentz force exerted on the flow is minimized once the fluid is compelled to move along magnetic streamlines. Surprisingly, however, examination of the result obtained for the velocity profile in figure 2 shows that the anticipated jet structure at large Hartmann numbers does not emerge. The profiles are observed to flatten for increasing M (see also Pai 1954) whilst conserving the volume flux through the pipe. The asymptotic limits $M \to \infty$ and $M \to 0$ are consistent with the behaviour for slug flow (uniform flow) and Poiseuille flow respectively. The tendency of the flow profiles to flatten at large M can be explained in terms of the dominating term present in the vorticity equations (2.13) and (3.18), namely the curl of the Lorentz force. At large M in the core of the flow, where the viscous terms are small, we approximately have

$$\nabla \times [(\boldsymbol{u} \times \boldsymbol{B}_0) \times \boldsymbol{B}] = 0. \tag{3.24}$$

From (3.2) and (3.17) this reduces to

$$u'(r) r^2 = 0, \tag{3.25}$$

and consequently $u = \text{const}$ in this limit. A physical explanation of this flow behaviour lies in a consideration of the nature of the axial pressure gradient, which can be written as

$$\frac{1}{N}\frac{\partial p}{\partial z} = -r^2 a_0(M) \int_{M^{\frac{1}{2}r}}^{M^{\frac{1}{2}}} \frac{\sinh(\frac{1}{2}\xi^2)}{\xi} \mathrm{d}\xi + \frac{a_0(M)}{M} \cosh(\tfrac{1}{2}Mr^2), \tag{3.26}$$

where the two terms on the right-hand side represent the electromagnetic and viscous contributions respectively. The following results are obtained for large M using (3.20):

$$\lim_{M\to\infty} \left.\frac{\partial p}{\partial z}\right|_{r=0} = O(\exp(-\tfrac{1}{2}M)), \quad \lim_{M\to\infty} \left.\frac{\partial p}{\partial z}\right|_{r=1} = O(M^2), \tag{3.27}$$

and where the pressure gradient in each case is balanced by contributions from the viscous term only. These results indicate that the pressure gradient vanishes along the neutral line of the magnetic field (along the pipe's axis) but rises sharply near the edges of the flow on account of the thin boundary layers which are $O(M^{-1})$ thickness. This behaviour corresponds to that exhibited by a slug flow that maintains unit flux.

3.3. *Two-dimensional neutral-point flow through a duct*

The physical set-up is similar to that described for the axisymmetric flow. In an analysis similar to that in §3.1 (Regirer 1960) one can show that only a magnetic stream function of the form

$$\chi(x,y) = x(h_0 y + h_1) + H_1(y) \tag{3.28}$$

allows the existence of unidirectional solutions, where h_0 and h_1 are constants and where $H_1(y)$ is the stream function for the induced component of magnetic field. The case $h_0 = 0$ corresponds to flow in a uniform transverse magnetic field or the much-studied Hartmann flow. In the present problem we consider the situation where $h_0 = -1$ and $h_1 = 0$ and specify the magnetic field according to

$$\begin{aligned} \boldsymbol{B} &= \nabla \times ([-xy + H_1(y)]\,\hat{z}) \\ &= (b(y) - x, y, 0), \end{aligned} \tag{3.29}$$

where $H_1'(y) = b(y)$ and $\hat{z}$ is normal to the plane of the flow. Consequently, the applied and induced magnetic fields have the form

$$\boldsymbol{B}_0 = (-x, y, 0), \quad \boldsymbol{b} = (b(y), 0, 0), \tag{3.30}$$

respectively. The unidirectional flow we seek to describe has the form

$$\boldsymbol{u} = (u(y), 0, 0), \tag{3.31}$$

whose component again satisfies a third-order differential equation obtained from the vorticity equation. The velocity interacts with the applied magnetic field component $\boldsymbol{B}_0$ to form a current distribution normal to the flow which gives rise to the induced component of magnetic field whose stream function $H_1(y)$ is related to $u(y)$ in a manner similar to the axisymmetric case (3.12), giving

$$H_1''(y) = b'(y) = -R_m\, u(y) y. \tag{3.32}$$

In the flows we consider it is assumed that there is no variation in the plane perpendicular to the flow. This assumption appears to be valid experimentally if the aspect ratio of the channel is very large. However, the sidewalls of the channel are important in determining the return path of currents induced in the flow and hence also the distribution of electric field. The various modes of operation of a given duct ranging from an e.m. brake to that of a generator depend on the conductivity of the sidewalls and are tabulated in Shercliff (1965, p. 148). For our particular purposes the sidewalls are assumed to be perfectly conducting with no electric field present, which ensures efficient brake operation. As it happens, the MHD flow considered in this paper passes through a symmetrical magnetic field distribution which produces zero net crosswise current and as a result is independent of the nature of the sidewalls.

These crosswise currents lie perpendicular to the plane of motion and are described by

$$\boldsymbol{j} = \boldsymbol{u} \times \boldsymbol{B}_0 = yu(y)\,\hat{z}, \tag{3.33}$$

using (3.30) and (3.31). When the velocity and magnetic field are specified according to (3.30) and (3.31) respectively, the Navier–Stokes equation linearizes according to (3.4) and has transverse and longitudinal pressure components similar to the axisymmetric situation. The equivalent form of (3.5) in two dimensions becomes

$$\frac{1}{N}\nabla p = yu(y)\,\nabla\chi(x, y) + \frac{1}{M^2}u''(y)\,\hat{x}. \tag{3.34}$$

Eliminating the pressure by taking the z-component of the curl of (3.34) results in a vorticity equation that is a differential equation in $u(y)$:

$$u''' - M^2 y(yu)' = 0. \tag{3.35}$$

Before solving (3.35) it is worth comparing it to the stream function–vorticity equation (2.13) which was derived on the basis that the induced field can be ignored.

Substituting the present forms of the magnetic field $\boldsymbol{B}_0$ and velocity $\boldsymbol{u}$ from (3.30) and (3.31) respectively into the nonlinear partial differential equation (2.13) yields (3.35) again. Clearly, the induced field contributes no rotational terms to the curl of the Lorentz force since it is parallel to the channel and is dependent on the transverse coordinate only.

We seek solutions to (3.35) for the range $0 \leqslant y \leqslant 1$ and by the symmetrical nature of (3.35) we can apply the result to the range $-1 \leqslant y \leqslant 0$. The boundary conditions are similar to those of the axisymmetric flow, namely

$$u(+1) = 0, \quad u'(0) = 0, \quad 2\int_0^{+1} u(y)\,\mathrm{d}y = 1, \tag{3.36}$$

which are the non-slip, symmetry and prescribed unit flux requirements respectively. Once again unit flux is specified rather than a pressure gradient so that a direct comparison may be easily made with corresponding profiles in the numerical study of flow in a magnetic field formed by a quadrupole arrangement of line currents (see §5). The transformation $Y = M^{\frac{1}{3}}y$ simplifies (3.35) to the following differential equation:

$$U''' - Y(YU)' = 0, \tag{3.37}$$

where $u(y) = U(Y)$. The general solution to (3.37) can be obtained by a one-step transformation to a more tractable second-order ordinary differential equation, Murphy (1960). Equation (3.37) is a specific case of the following general equation:

$$U''' + 2f(Y)\,U' + f(Y)\,U = 0, \tag{3.38}$$

where $f(Y) = -\frac{1}{2}Y^2$ in this example. If we now solve

$$g'' + \tfrac{1}{2}f(Y)\,g = 0, \tag{3.39}$$

then the solution to (3.38) is given by

$$U(Y) = ag_1^2(Y) + bg_1(Y)\,g_2(Y) + cg_2^2(Y), \tag{3.40}$$

where g_1, g_2 are the complementary solutions of (3.39).

The general solution for the velocity becomes

$$u(y) = y[AI_{\frac{1}{4}}^2(\beta y^2) + BI_{\frac{1}{4}}(\beta y^2)\,I_{-\frac{1}{4}}(\beta y^2) + CI_{-\frac{1}{4}}^2(\beta y^2)], \tag{3.41}$$

where $\beta = \frac{1}{4}M$ and A, B, C are constants. Despite appearances the modified Bessel functions $I_{\frac{1}{4}}^2(\beta y^2)$ and $I_{-\frac{1}{4}}^2(\beta y^2)$ are odd functions of y and care must be taken to ensure that symmetry is applied properly over the range $-1 \leqslant y \leqslant 0$. If we impose the boundary conditions (3.36) then we can specify the velocity up to a multiplicative constant $A(\beta)$, which is determined by the condition of unit flux passing through any cross-section of the channel:

$$u(y) = A(\beta)y[I_{\frac{1}{4}}^2(\beta)\,I_{-\frac{1}{4}}^2(\beta y^2) - I_{-\frac{1}{4}}^2(\beta)I_{\frac{1}{4}}^2(\beta y^2)], \tag{3.42}$$

where

$$A(\beta) = \left[I_{\frac{1}{4}}^2(\beta)\int_{-1}^{1} \xi I_{-\frac{1}{4}}^2(\beta\xi^2)\,\mathrm{d}\xi - I_{-\frac{1}{4}}^2(\beta)\int_{-1}^{1} \xi I_{\frac{1}{4}}^2(\beta\xi^2)\,\mathrm{d}\xi\right]^{-1}. \tag{3.43}$$

The induced magnetic field follows from application of Ohm's law using (2.8) and (3.33) once we have established the following indefinite integral relationship:

$$\int^z \zeta^{\frac{1}{2}} I_{\pm\frac{1}{4}}^2(\zeta)\,\mathrm{d}\zeta = z^{\frac{3}{2}}(I_{\pm\frac{1}{4}}^2(z) - I_{\mp\frac{3}{4}}^2(z)), \tag{3.44}$$

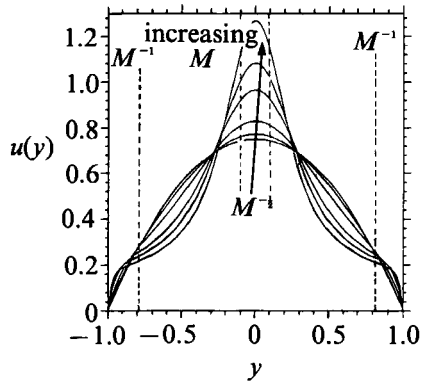

FIGURE 3. Two-dimensional velocity profiles at various Hartmann numbers with unit flux.

and so

$$b(y) = -R_{\mathrm{m}} A(\beta) y^3 [I^2_{\frac{1}{4}}(\beta) I^2_{-\frac{1}{4}}(\beta y^2) - I^2_{\frac{1}{4}}(\beta y^2) I^2_{-\frac{1}{4}}(\beta) - I^2_{\frac{1}{4}}(\beta) I^2_{\frac{3}{4}}(\beta y^2) + I^2_{-\frac{1}{4}}(\beta) I^2_{-\frac{3}{4}}(\beta y^2) + I^2_{\frac{1}{4}}(\beta) I^2_{\frac{3}{4}}(\beta) - I^2_{-\frac{1}{4}}(\beta) I^2_{-\frac{3}{4}}(\beta)], \quad (3.45)$$

with the boundary condition that $b(\pm 1) = 0$ for the reasons given in the previous section. The equation for the pressure gradient in (3.34) may be integrated in a manner analogous to the axisymmetric case to give

$$p(x, y) = -kx - \frac{N}{2R_{\mathrm{m}}} b^2(y) + \frac{N}{R_{\mathrm{m}}} x b(y), \quad (3.46)$$

where we have used (3.32). The constant k can be found from (3.34) and (3.43) and denotes the constant background pressure gradient. Once again the pressure depends on the transverse coordinate y at large $\pm x$ in contrast to Poiseuille flow where the pressure is uniform across the channel. As explained earlier, this is a consequence of the unbounded extent of the magnetic field.

The analysis involved in both the two-dimensional and axisymmetric flows is similar and one is tempted to infer that the resulting behaviour of the two flows is also likely to be similar. That this is not so is demonstrated by the contrasting asymptotic behaviour of the two flows at large values of M. In this limit both flows are governed in the core by

$$\nabla \times \{\boldsymbol{j} \times \boldsymbol{B}\} = 0 \quad \text{or in two dimensions} \quad \boldsymbol{B} \cdot \nabla \boldsymbol{j} = 0 \quad (3.47)$$

(see also (3.25)). Using the expressions for $\boldsymbol{j}$ and $\boldsymbol{B}$ from (3.33) and (3.29) respectively one deduces that in this limit

$$(yu)' = 0 \quad \text{or} \quad u \sim \frac{1}{y}. \quad (3.48)$$

Clearly, therefore, the two-dimensional flow exhibits a jet-like structure centred on $y = 0$ in contrast to the slug profile of axisymmetry. This behaviour is clearly illustrated by the profiles in figure 3. In both cases the governing physical principle is that the curl of the Lorentz force is approximately zero for large M and this implies differing constraints on the velocity in the different geometries. Arguments similar to those employed in the case of axisymmetry show that the pressure gradient along the

neutral line ($y = 0$) is balanced by the viscous term present in (3.34). Inspection of figure 3 shows that boundary layers form near the axis of the channel $y = 0$ which from (3.37) have thickness $O(M^{-\frac{1}{2}})$. Consequently, in contrast to the axisymmetric case the longitudinal pressure gradient is not small but is balanced by the boundary-layer derivatives present in the viscous term. The boundary layers near the walls of the channel $y = \pm 1$ are of $O(M^{-1})$ thickness as is usual for Hartmann-like flows.

4. Numerical study of two-dimensional flows in non-uniform magnetic fields

In this section a numerical formulation for modelling two-dimensional MHD duct flows in the presence of a non-uniform magnetic field is presented. The full set of MHD equations are solved subject only to the assumption of small magnetic Reynolds number (i.e. that the induced magnetic field component of (2.2) is negligibly small compared to the imposed field). This assumption leads to an uncoupling of the magnetic field and velocity so that the steady motion can be described by the stream function–vorticity equation (2.13). In two dimensions we can simplify (2.13) to a single scalar equation by introducing a stream function $\boldsymbol{u} = \boldsymbol{\nabla} \times (\psi \hat{\boldsymbol{z}})$ ($\hat{\boldsymbol{z}}$ normal to the plane of flow) to give

$$\frac{1}{R}\nabla^2\omega - (\boldsymbol{u}\cdot\boldsymbol{\nabla})\omega = \boldsymbol{\nabla} \times [(\boldsymbol{u} \times \boldsymbol{B}_0) \times \boldsymbol{B}_0]\cdot\hat{\boldsymbol{z}}$$
$$= -N[(\boldsymbol{B}_0\cdot\boldsymbol{\nabla})^2\psi], \tag{4.1}$$

where $\omega = -\nabla^2\psi$. This equation forms the basis for modelling a liquid-metal flow through a specified non-uniform magnetic field $\boldsymbol{B}_0$. Most other numerical studies have tended to consider the effect of a non-uniform field normal to the plane of flow using either a finite-element analysis (Yugawa & Masuda 1982), or a finite-difference analysis of the coupled Navier–Stokes and Maxwell equations (Ramos & Winowich 1986). Gel'fgat, Peterson & Shcherbinin (1978*a*, *b*) also employed a finite-difference analysis based upon the stream function–vorticity equation (4.1) but with the simplifying assumption that the magnetic field possessed a single component normal to the plane of flow. The numerical scheme employed to solve (4.1) is based upon a highly accurate method which has proven effective for classical hydrodynamical problems.

4.1. *Description of numerical scheme*

The technique employed to solve the vorticity equation (4.1) is based upon an iteration scheme using the 'Compact explicit h^4 finite difference approximations to operators of the Navier–Stokes type' by Dennis (1985) and was the culmination of earlier work on accurate numerical representations of partial differential equations (Dennis & Hudson 1979, 1980). The 'Compact h^4' approach is based upon the use of integrating factors and combinations of one-dimensional problems. However, the same set of equations can be obtained using the two-dimensional extension of the Numerov method for expanding the ordinary differential equation $f'' = g$ in finite-difference form. For further details of the numerical scheme the reader is referred to Dennis (1985) and Kenny (1990).

The h^4 approximation to $\nabla^2\psi_0 = -\omega_0$ represents a convenient starting point in the scheme, namely

$$4(\psi_1+\psi_2+\psi_3+\psi_4)+\psi_5+\psi_6+\psi_7+\psi_8-20\psi_0 = -\tfrac{1}{2}h^2(\omega_1+\omega_2+\omega_3+\omega_4+8\omega_0)+O(h^6), \tag{4.2}$$

using a cubic array of grid points:

$$\begin{array}{ccc} 6\cdot & 2\cdot & 5\cdot \\ 3\cdot & 0\cdot & 1\cdot \\ 7\cdot & 4\cdot & 8\cdot \end{array}$$

In order to obtain a similarly accurate representation of the stream function–vorticity equation with no forcing term present we apply the Numerov method to the following two equations:

$$\omega_{xx} - u\omega_x = r = -(\omega_{yy} - v\omega_y), \tag{4.3}$$

where (u, v) are the components of the velocity. The resulting approximation to (4.3) in terms of the compact tridiagonal scheme gives

$$c_1\omega_1 + c_2\omega_2 + c_3\omega_3 + c_4\omega_4 - (c_0 + c_0^*)\omega_0 + E_0 + D_0 = 0. \tag{4.4}$$

The coefficients c_0, c_0^*–c_4 contain partial derivatives of the velocity with respect to x and y. The coefficients E_0 and D_0 are both $O(h^4)$ and it remains to evaluate them correctly without introducing any terms greater than $O(h^6)$. Full details of these coefficients are given in Dennis (1985).

Stability of the iteration procedure used to calculate ω_0 is dependent upon the diagonal dominance of the scheme, i.e. the associated matrix of the nine-point star centred on any grid point contains positive definite diagonal elements for all values of the velocity and its derivatives. Since normally the velocity components u and v in (4.3) are multiplied by a Reynolds number factor (here omitted for the sake of clarity), which may be fairly large, diagonal dominance of the scheme could be lost. For stability purposes this is an undesirable feature and O. Tutty (1988, personal communication) circumvented this possibility by reducing the situation to that of a diagonally dominant matrix plus an additive correction (known later as the 'RHS correction'). Following Tutty, therefore, the scheme of (4.4) is reduced to the form,

$$d_1\omega_1 + d_2\omega_2 + d_3\omega_3 + d_4\omega_4 - d_0\omega_0 + F_0 = 0, \tag{4.5}$$

where $d_n > 0$ $(n = 0, 1, 2, 3, 4)$ and,

$$d_0 = d_1 + d_2 + d_3 + d_4 + 8. \tag{4.6}$$

This derives from a rearrangement of terms in E_0 and D_0 and the coefficients of ω_0–ω_4 in (4.4). The coefficients d_n involve only values of u and v at (x_0, y_0) whilst those terms in F_0 contain values of u, v at the corner points $5, 6, 7, 8$ together with any terms involving $(\partial u/\partial x)_0$, $(\partial^2 u/\partial x^2)_0$, $(\partial v/\partial y)_0$ and $(\partial^2 v/\partial y^2)_0$ in the coefficients of $\omega_1, \omega_2, \omega_3$ etc.

Inclusion of a generalized body force term $R(x, y)$ on the right-hand side of the stream function–vorticity partial differential equation in (4.3) is relatively easy to implement. Proceeding in exactly the same way as before one finds,

$$\sum_{n=1}^{4} d_n\omega_n - d_0\omega_0 + F_0 + G_0 = 0, \tag{4.7}$$

where the d_n $(n = 0, 1, 2, 3, 4)$ and F_0 are the same as before and G_0 includes the extra body force terms in the following manner:

$$G_0 = -h^2[(1 - \tfrac{1}{2}hu_0)R_1 + (1 - \tfrac{1}{2}hv_0)R_2 + (1 + \tfrac{1}{2}hu_0)R_3 + (1 + \tfrac{1}{2}hv_0)R_4 + 8R_0)]. \tag{4.8}$$

4.2. *Lorentz force*

Up to this point a numerical procedure has been described which shows how to construct a representation of the stream function–vorticity equation (4.3) accurate to $O(h^4)$. This allows us to solve accurately hydrodynamic problems with a specified body force distribution, examples of which are given by Dennis (1985). The novel application of this numerical scheme to the solution of the MHD equations describing two-dimensional channel flow presents several complications which need to be overcome. The first concerns the nature of the magnetic body force term appearing in (4.1). The rotational component of the Lorentz force $-N\{(\boldsymbol{B}_0\cdot\nabla)^2\psi\}$ depends on present fluid behaviour in the form of u, v and ω. These extra terms must be included in Tutty's scheme (4.5)–(4.6) without incurring any loss of accuracy or disruption to the original diagonal dominance of the scheme. The expansion of this rotational term becomes

$$-N(\boldsymbol{B}_0\cdot\nabla)^2\psi = N\Big[-B_{0_x}^2 v_x + B_{0_y}^2 u_y + B_{0_x}B_{0_y}(u_x - v_y) - v\Big(B_{0_x}\frac{\partial B_{0_x}}{\partial x} + B_{0_y}\frac{\partial B_{0_x}}{\partial y}\Big) + u\Big(B_{0_x}\frac{\partial B_{0_y}}{\partial x} + B_{0_y}\frac{\partial B_{0_y}}{\partial y}\Big)\Big], \quad (4.9)$$

where $\boldsymbol{B}_0 = (B_{0_x}, B_{0_y}, 0)$ and $(u, v) = (\psi_y, -\psi_x, 0)$.

The quantities u and v appearing in (4.9) are already evaluated to $O(h^4)$ and it remains to estimate the derivatives of u and v to a similar order of accuracy. Consequently, the general expression for the forcing term (4.9) can be found and included in Tutty's scheme according to (4.7) and (4.8). It is important to identify any terms arising from the force term G_0 in (4.8) which might affect the diagonal dominance of Tutty's scheme. It is found that the choice of representing the rotational Lorentz force term (4.9) in terms of the elements of the compact scheme shown earlier results in a positive contribution to the diagonal dominance of Tutty's scheme (4.5)–(4.6) in the following way:

$$[d_1 + \tfrac{4}{3}h^2M^2B_{0_x}^2]\omega_1 + [d_2 + \tfrac{4}{3}h^2M^2B_{0_y}^2]\omega_2 + [d_3 + \tfrac{4}{3}h^2M^2B_{0_x}^2]\omega_3 + [d_4 + \tfrac{4}{3}h^2M^2B_{0_y}^2]\omega_4 - [d_0 + \tfrac{8}{3}h^2M^2(B_x^2 + B_y^2)_0]\omega_0 + F_0 + \tilde{G}_0 = 0, \quad (4.10)$$

where $\tilde{G}_0$ is the suitably modified form G_0 in (4.7) and where the components of the magnetic field $\boldsymbol{B}_0$ are evaluated at index point 0. The remaining magnetic terms contained in $\tilde{G}_0$ are a mixture of velocity and stream-function values and 'off-diagonal' vorticity values. A possible breakdown of the scheme occurs if the new terms in the 'RHS correction' matrix, $F_0 + \tilde{G}_0$ become of the same order of magnitude as those of the diagonal coefficients for large values of M. A numerical breakdown in this sense means that the scheme will not converge and is a consequence of the fact that thin boundary layers have formed, for example, near to the channel walls, which cannot be resolved by the chosen grid spacing. The gradients of quantities in the vicinity of such layers become very large and hence the diagonal dominance of the scheme in (4.10) may be upset.

5. Boundary conditions

The general flow situation which we wish to model consists of a specified two-dimensional duct flow encountering a region of non-uniform magnetic field which acts for a certain length of channel. Assuming the channel is long enough, the flow

then emerges from this region and adjusts to the Poiseuille profile over the remaining 'field-free' length of channel. A diagram showing the general flow situation which is modelled is given in figure 1. The total length of duct over which the magnetic field acts on the flow and the length associated with the recovery of the flow to Poiseuille type is modelled as a rectangular box. This specified rectangular region is a consequence of the elliptical nature of the stream function–vorticity equation, (4.1), and has boundary conditions applied to each of its sides. We must now describe a suitable set of boundary conditions which model reality as closely as possible. At the input, the stream function ψ and vorticity ω are independently specified but in the neutral-point flow examined later are usually associated with the Poiseuille entry conditions. Downstream, at the exit to the domain, the flow has fully recovered from the disturbance and is now of Poiseuille type. The impetus for the flow is provided by the condition that unit flux passes through the channel such that $\psi(+1) = 1$ and $\psi(-1) = 0$, where $y = \pm 1$ denotes the walls of the duct. Also, the non-slip condition at the sidewalls implies that $\psi_x(\pm 1) = \psi_y(\pm 1) = 0$.

Implementing the boundary conditions into a numerical scheme requires certain assumptions and simplifications if the scheme is to work effectively. For example, in the neutral-point flows considered later the magnetic field is generated by a quadrupole distribution of line currents external to the duct which decays with increasing distance along the duct. The numerical scheme fixes an effective range for the field and ensures a smooth transition to the 'field-free' region. A less strict application of the downstream Poiseuille exit conditions is also required to make the numerical scheme work efficiently. Inevitably, any numerical code introduces errors which, when confined to a well-defined region, tend to propagate backwards and forwards inside that region. The Poiseuille exit conditions are therefore relaxed in the numerical model to prevent the accumulation of these error waves inside the rectangular section of channel. The numerical exit conditions used, namely $\psi_{xx} = \omega_{xx} = 0$, permit the flow to be at most weakly linear in x and provide a means of ensuring that the numerical scheme used to model the flow (§4) will converge for a range of parameters.

The implementation of the boundary conditions is an important aspect in determining the stability of the numerical scheme (4.10). As is usual with channel flows, complications arise near the boundaries and variables are not guaranteed to be evaluated there to the same order of accuracy as in the main flow region. This applies particularly to the estimation of wall vorticity values at $y = \pm 1$, which are found to critically determine the overall rate of convergence of the numerical scheme. In this case we use a polynomial expansion using four grid values of ψ involving known boundary conditions so that the approximation of $\psi_{yy} (= -\omega)$ is correct to $O(h^4)$. However, at large Hartmann numbers the possibility of boundary-layer formation requires that the number of grid points used in the estimation of ω is not greater than the number of grid points spanning any boundary layers. It was assumed that where the magnetic field was nearly transverse to the channel wall the layer thickness was $O(M^{-1})$, which enabled an estimate to be made of the suitability of modelling the flow with the fixed grid scheme of 32×512 points.

6. Flow through non-uniform magnetic fields containing a neutral point

The numerical procedure outlined in §4 is now applied to model a fully developed two-dimensional channel flow impinging upon a region of non-uniform magnetic field. The initial entry conditions are taken to be those of Poiseuille, assuming that

sufficient length of duct exists for the flow to settle down prior to entering the region of non-uniform field. In practical situations the flow will frequently emerge from a receptacle (e.g. tun dish) with a profile that is unlikely to be of Poiseuille type. A 'slug' (uniform) input might be considered a more suitable entry condition; however, this introduces additional complications owing to the hydrodynamic evolution of the slug component itself (Van Dyke 1970). For a more extensive consideration of MHD flows with 'slug' entry conditions the reader is referred to Kenny (1990). It was observed in later numerical experiments that the pressure and volume flux results were not significantly altered by using a slug input, because it was the 'excess' pressure over and above that of the basic hydrodynamic behaviour that mattered. Consequently, for ease of computation a Poiseuille input was applied to the channel.

The case study employs a quadrupole magnetic field derived from four line currents external to the duct. In practical situations the effective range of the magnetic field is limited since it falls off rapidly with increasing distance along the duct. The corresponding numerical model switches on the magnetic field to an initial low value which acts for a specified length of duct and is then turned off from a suitably low value, allowing the flow to settle down again over the remaining length L of channel. An estimate can be made of this length L, which is useful for predicting a sufficiently long standard length of duct which may be employed in all the numerical experiments. Any disturbance introduced into a flow, in this case of a magnetic nature, tends to create a non-uniform distribution of vorticity which decays according to a timescale τ, given by

$$\tau \sim a^2/\nu, \tag{6.1}$$

where a is a characteristic lengthscale of the disturbance, which in this case corresponds to the width of channel, and where ν is the kinematic viscosity. The timescale τ can be estimated by considering the combination of a typical x-component of velocity U_0 and the length L over which the vorticity distribution decays, $\tau \sim L/U_0$. The two expressions for τ can be combined to provide an estimate for L:

$$L \sim a^2 U_0/\nu = aR, \tag{6.2}$$

from the definition of R in (2.12). This expression for L provides a rough estimate for the length of duct required sufficient to model all the flows considered and was taken to be 16 times the width. The effect of varying the channel length by a few widths was investigated and showed that for the range of R values considered the Poiseuille profiles at the exit changed by a negligible amount. It was concluded, therefore, that ample channel length had been allocated for the flow profiles to settle down to Poiseuille type. The extent of channel over which the magnetic field was permitted to act was six channel widths. A sketch of the arrangement including details of the boundary conditions is shown in figure 1.

6.1. *Quadrupole magnetic field*

The quadrupolar arrangement of line currents gives rise to a magnetic stream function χ of the form

$$\begin{aligned}\chi \propto \log[(d-y)^2+(2a-x)^2]-\log[(d-y)^2+(2a+x)^2]\\ +\log[(d+y)^2+(2a+x)^2]-\log[(d+y)^2+(2a-x)^2],\end{aligned} \tag{6.3}$$

where d is the distance of any line current from the axis of the channel. A constant of proportionality is implied in (6.3) which is chosen so that $\chi \sim xy$ near to the

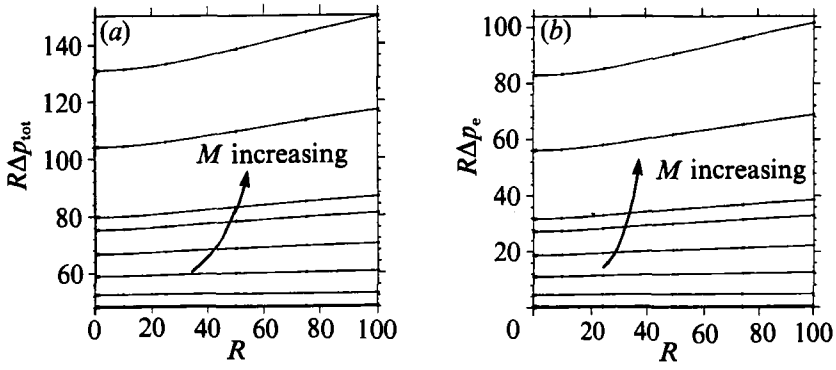

FIGURE 4. Plots of (*a*) total pressure drop and (*b*) excess pressure drop against R for various increasing values of the Hartmann number.

neutral point and allows easy comparison of this study with that involving the extended neutral point (3.29) discussed in §3. This factor is quite large, $O(10)$ for $a = 2$ and $d = 1.5$, and should really be incorporated into the definition of the Hartmann number in (2.11) for this flow. However, rather than change the definition of M it should be simply be borne in mind that the effective values of M are larger than those indicated in the figures.

6.2 *Analysis of pressure results at fixed volume flux*

At the end of each computation on a given flow, the Hartmann number M, Reynolds number R, interaction parameter N, pressure drop across the ends of the duct Δp_{tot} and 'excess' pressure drop Δp_e were recorded for unit flux. The concept of 'excess' pressure drop was introduced to measure the pressure drop over and above that due to the Poiseuille component of the flow. The behaviour of the pressure drops shown in figures 4 and 5 is computed from (2.9) which is rewritten as

$$\nabla p = -\tfrac{1}{2}\nabla(\boldsymbol{u}\cdot\boldsymbol{u}) + \boldsymbol{u}\times\boldsymbol{\Omega} + N\boldsymbol{j}\times\boldsymbol{B}_0 + \frac{1}{R}\nabla^2\boldsymbol{u}. \tag{6.4}$$

Integrating the x-component of (6.4) between the ends of the channel and assuming that at the exit of the channel there is Poiseuille flow (as it is at the input) gives

$$R\Delta p_{tot} = R\int_{x_0}^{x_1} v\omega\,dx + M^2\int_{x_0}^{x_m} j\chi_z\,dx + \int_{x_0}^{x_1}\nabla^2 u\,dx, \tag{6.5}$$

where x_0, x_m and x_1 denote the entrance of the channel, the end of the magnetic field region and the channel exit respectively, and where (u, v) are the components of the velocity, j is the z-component of current and $-\chi_z$ is the y-component of the magnetic field from (6.3). The boundary conditions imposed upon the flow imply that Δp_{tot} does not vary with position across the duct and we can select any convenient pathway between the ends of the channel with which to evaluate Δp_{tot}. The axis of the channel ($y = 0$) is a convenient location to calculate Δp_{tot} since the flow is symmetrical and $v = 0$ there, which eliminates the first integral in (6.5), whilst the second vanishes with $y = 0$ due to the form of $\boldsymbol{B}_0$ derived from (6.3). Equally, we may integrate along the walls of the duct since $\boldsymbol{u} = 0$ there and once again the same two integrals vanish.

Figure 4(*a*) plots several curves of $R\Delta p_{tot}$ against R for an increasing series of M-values varying from about $M = 0$ to 35, all at fixed unit flux. The curves exhibit both

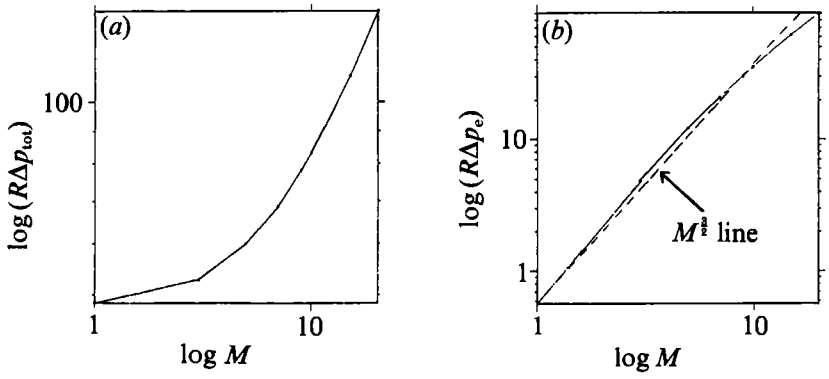

FIGURE 5. Log-log plots of (*a*) total pressure drop and (*b*) excess pressure drop against the Hartmann number at a fixed value of $R = 50$. The gradient of the asymptotic straight line is approximately 0.60.

an increasing intercept with the pressure axis and a greater limiting linear gradient with increasing magnetic influence. A cross-section of figure 4(*a*) which records the variation of the quantity $R\Delta p_{\text{tot}}$ plotted as a log-log relationship against M for $R = 50$ is shown in figure 5(*a*). Since the values of the parameters M, N and R are mostly $O(1)$ it appears to be difficult to sort out the magnetic from the viscous behaviour; consequently, in an attempt to separate some of the viscous and magnetic effects the idea of 'excess' pressure was introduced, which differed from the total pressure drop by simply subtracting the pressure drop due to a Poiseuille flow over a similar length of channel. Figure 4(*b*) shows excess pressure drop against R for increasing M-values. The graph corresponding to figure 5(*a*) but involving the excess pressure Δp_{e} (figure 5(*b*), indicates the linear nature of the relationship $\log R\Delta p_{\text{e}}$ against $\log M$ for large values of M, resulting from the definition of excess pressure.

An asymptotic study of the stream function–vorticity equation in the limit of large M may be carried out by assuming that the flow forms a jet-like structure along the axis of the channel. This behaviour was predicted by a previous analytical observation in (3.48) for an extended magnetic neutral point. In this narrow region the y-component of velocity is zero from symmetry conditions and the derivatives of quantities in the x-direction are assumed to be much smaller than those in the y-direction. Consequently, the boundary-layer equation derived from (2.13) consists of a balance between the viscous and magnetic terms, so that

$$\frac{1}{R}\psi_{yyyy} \sim -N(\boldsymbol{B}_0 \cdot \nabla)^2 \psi, \tag{6.6}$$

which applies in the neighbourhood of the neutral line and where we have used (2.12) and the fact that $(\boldsymbol{B}_0 \cdot \nabla) \sim x\partial/\partial x + y\partial/\partial y$ is $O(1)$ along the axis from the form of $\boldsymbol{B}_0$ derived from (6.3). The order-of-magnitude relation in (6.6) applies all along the magnetic neutral line despite the algebraic decay, which does not affect the nature of the derivatives appearing on the right-hand side of (6.6). If we scale the y-coordinate according to,

$$y = \delta Y, \quad \delta \ll 1, \tag{6.7}$$

where $Y = O(1)$, then substituting into (6.6) and balancing the principal terms gives

$$\delta = O(M^{-\frac{1}{2}}). \tag{6.8}$$

This compares with earlier analytical work on extended two-dimensional neutral-point flows which suggested the development of a jet structure for large values of M in (3.48), with a width $O(M^{-\frac{1}{2}})$ from (3.35) and (3.37).

The asymptotic behaviour of $R\Delta p_e$ against M for fixed R and volume flux is now investigated and compared with what is observed numerically. Evaluation of $R\Delta p_e$ along the neutral line ($y = 0$) gives,

$$R\Delta p_e = \int_{x_0}^{x_1} \nabla^2(u - u_{\text{Pois}})|_{y=0}\, dx, \tag{6.9}$$

which is obtained using the symmetry condition $v|_{y=0} = 0$ in (6.5) and where u_{Pois} denotes the Poiseuille component of velocity. The dominating behaviour of the right-hand side term in (6.9) at large M is given by

$$\lim_{M\to\infty} R\Delta p_e \sim (\tilde{u}/\delta^2)(x_1 - x_0) \sim M\tilde{u}(x_1 - x_0), \tag{6.10}$$

where $\tilde{u}$ is an estimate of the jet velocity. The specified volume flux Q may be related to $\tilde{u}$ if certain assumptions about the structure of the flow are made. Firstly, we assume that the jet velocity is approximately constant across the central boundary layer of thickness $O(M^{-\frac{1}{2}})$. The contribution, Q_J, to the total volume flux from this region is estimated as

$$Q_J \sim \tilde{u}M^{-\frac{1}{2}}. \tag{6.11}$$

Secondly, across the core of the flow it is assumed that the x-component of velocity behaves as $\sim 1/y$ according to (3.48). Matching the core profile to that near the axis and integrating across the core yields an approximate expression for the volume flux, Q_C, flowing in this region:

$$Q_C \sim \tilde{u}M^{-\frac{1}{2}} \log M. \tag{6.12}$$

Near to the walls of the channel there are Hartmann-like boundary layers of thickness $O(M^{-1})$. Matching the sidewall profile with that in the core, $\tilde{u}M^{-\frac{1}{2}}/y$, enables us to estimate the volume flux Q_H flowing in these layers, giving

$$Q_H \sim \tilde{u}M^{-\frac{3}{2}}. \tag{6.13}$$

Adding the estimates of contributions to the total volume flux Q at large M from (6.11)–(6.13) gives

$$Q \sim \tilde{u} \log M M^{-\frac{1}{2}}. \tag{6.14}$$

Equations (6.10) and (6.14) can be combined to provide an estimate for the asymptotic behaviour of $R\Delta p_e$ at large M for fixed Q, to give

$$\lim_{M\to\infty} R\Delta p_e \sim \frac{QM^{\frac{3}{2}}}{\log M}. \tag{6.15}$$

In figure 5(*b*) it appears that the gradient of the asymptotic straight line of $\log R\Delta p_e$ against $\log M$ is 1.46, which agrees well with the theoretical prediction $\sim M^{\frac{3}{2}}$ for the dominating magnetic pressure contribution in Δp_e, (6.15).

6.3. *Analysis of volume flux results at fixed pressure drop*

In practical situations involving a tun dish it is more convenient to maintain a constant hydrostatic head of metal and to measure variations in the mass or volume flux of the exit flow for various magnetic field strengths. In order to do this

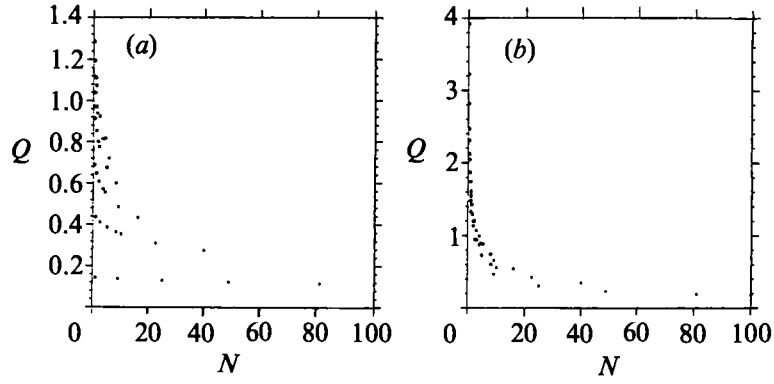

FIGURE 6. Plots of volume flux Q against interaction parameter N at (a) constant total pressure drop, and (b) constant excess pressure drop.

numerically, from the data collected at various fixed values of the volume flux, advantage is taken of the fact that similar flows result when ψ is scaled by λ, R by $1/\lambda$ and the pressure drop by a factor λ^2. The latter condition can be expressed as

$$\Delta p(M,R,Q) = (1/\lambda^2)\Delta p(M,R/\lambda,\lambda Q), \tag{6.16}$$

obtained from rescaling (6.5). This relation was checked numerically by scaling a known ψ,ω at a given M and R to give $\lambda\psi$, $\lambda\omega$, M, R/λ and substituting back into the scheme to verify that it remained a solution. The resulting pressure drop was compared with that obtained previously and observed to satisfy (6.16). The relationship in (6.16) allows the data to be inverted so that the variation of the volume flux Q with N (interaction parameter) may be examined at a given pressure drop. The results shown in figure 6(a) indicate that no simple correlation exists between Q and N when the total pressure drop is fixed. In contrast, the plot shown in figure 6(b) at fixed Δp_e appears to outline a curve which would be more clearly plotted as a log-log relationship between Q and N. The former behaviour is no doubt due to the inclusion of the viscous contribution to the pressure drop whilst the latter mostly includes the magnetic component of pressure. In order to examine such behaviour we consider an excess pressure drop evaluated along the magnetic neutral line (axis of the channel $y = 0$) similarly to (6.9). The right-hand side of (6.9) is evaluated at various values of Q, R, M and N keeping Δp_e fixed. In the case of large M it was mentioned before that a boundary layer of thickness $O(M^{-\frac{1}{2}})$ forms near to the axis of the channel, (6.8). Using the asymptotic relationship derived in (6.15) but keeping Δp_e fixed we find

$$\lim_{M\to\infty} Q \sim N^{-\frac{3}{4}} R^{\frac{1}{4}} \log(NR). \tag{6.17}$$

The asymptotic behaviour of Q in (6.17) therefore predicts a dependency on both N and R. However, the corresponding numerical plot of $\log Q$ versus $\log N$, shown in figure 7, indicates the approximate relation $Q \sim N^{-\frac{1}{4}}$, independent of R. For the range of values of Q and N considered it seems likely that these values fall coincidentally on the curve $Q \sim N^{-\frac{1}{4}}$. A deeper investigation of the parameter space would reveal a fully three-dimensional dependence on Q, N and R. That this is likely can be observed in figure 6(b), where there is an increasing scatter of points for increasing N, signifying a possible transition from the inertial dominance of the flow. Unfortunately, the constraints of computer storage upon the numerical code prevented

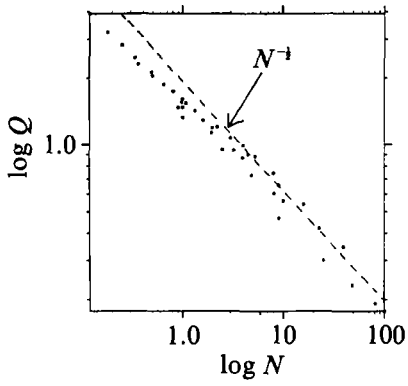

FIGURE 7. Log-log plot of volume flux Q against interaction parameter N for fixed excess pressure drop. Gradient of asymptotic straight line is approximately -0.46.

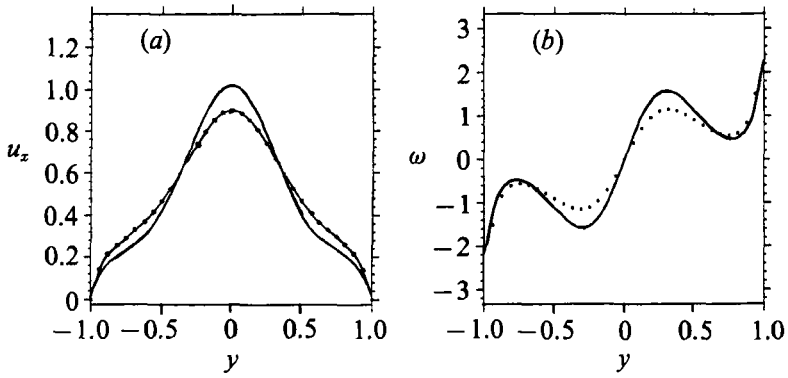

FIGURE 8. Profile of (*a*) of the x-component of velocity and (*b*) the vorticity at the geometric centre of the four wires (—) compared with the unidirectional analytical solution of an extended neutral point (·····)

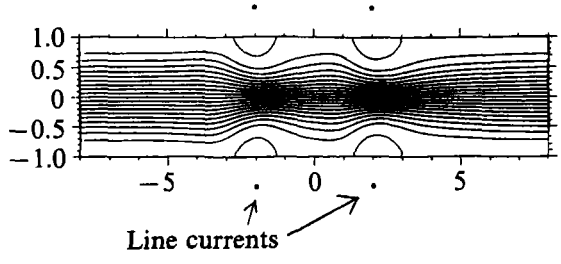

FIGURE 9. Plot of streamlines for $M = 15$, $R = 75$.

a deeper investigation into the asymptotic regime of this flow. However, previous experimental and numerical studies have mostly looked at the behaviour of flows for which $M, N \to \infty$, e.g. Holroyd & Hunt (1978), so that the case of $N = O(1)$ has novel implications. Indeed, the extent to which the flow rate diminishes with field strength has practical application in the factory environment where flow control devices tend to function with a constant hydrostatic head and may operate in the $N = O(1)$ regime.

6.4. *Comparison of analytical and numerical results*

The definitive test of the linear theory of two-dimensional neutral-point flows (§3) can now be observed in figures 8 and 9. A comparison of the x-component of velocity obtained numerically in a cross-section through the neutral point and that derived

analytically is shown in figure 8(*a*). A similar comparison for vorticity is shown in figure 8(*b*). The good agreement of results does not apply on either side of the neutral point as, farther downstream for example, disparities between the two flows emerge once the fully developed flow undergoes flow reversal at the walls. This behaviour is demonstrated in figure 9 which traces the streamlines throughout the channel for $M = 15$ and $R = 75$. The parallel streamlines at input are increasingly disturbed by the curvature of the magnetic field lines and some of the flow undergoes reversal opposite to each of the line currents. It will also be observed that in the vicinity of the neutral point the flow is non-symmetric about the line $x = 0$ which is an expected feature of the stream function–vorticity partial differential equation (4.1). Finally, after passing through the magnetic disturbance the streamlines readjust over a length of duct according to (6.2) and become parallel once again.

7. Concluding remarks

In this paper we have shown that unidirectional flow occurs in the vicinity of a local neutral point when a fully nonlinear flow of liquid metal encounters a region of quadrupole magnetic field. The corresponding linear problem (§3) examines unidirectional flow through a neutral point extending throughout a given flow. The good agreement of results does not apply on either side of the neutral point as, farther downstream for example, disparities between the two flows emerge once the fully developed flow undergoes flow reversal at the walls. The regions of flow reversal occur near each line current and become more pronounced with increasing M, corresponding to a stronger pinching effect exerted on the flow.

A second feature of the numerical study concerned the nature of the Q versus N graph, at constant excess pressure, which provides information on the quantity of fluid braked under certain conditions and enables further predictions to be made. Even though turbulence is often present in most flows and the value of R rather uncertain, some estimates can be made if the magnetic forces dominate and N is known, which is quite often the case with practical liquid-metal flows.

The numerical model discussed in this paper can be used to solve many other types of MHD flows; further examples may be found in Kenny (1990). For example, it is observed that two line currents placed symmetrically above and below the duct yield similar flow behaviour to that observed using four wires. A more instructive problem examines duct flow impinging upon a region of field generated by a single line current. In this problem the boundary conditions perpendicular to the plane of flow (or direction of no variation) are important in determining the presence or otherwise of an electric field. In order to optimize the braking action of the flow the walls are assumed to be perfectly conducting to provide a return path for the currents induced in the flow. The chief difference in this study is the effect of the wall (farthest from the line current) on the flow compared to the previous symmetrical flow problems. At large values of M a jet structure of finite width and extent develops along this particular wall. The reason for the formation of this well-defined jet region can be explained by the nature of the magnetic components in that region. The two field components along the wall provide terms of equal weight when incorporated into the asymptotic form of (4.1). Consequently, a boundary-layer scaling for the extent of the region along the duct wall is required in addition to that characterizing the width.

The development of a highly accurate numerical code to solve two-dimensional MHD duct flows through non-uniform fields (varying in the direction of flow)

provides a powerful means of understanding the behaviour of these flows in various parameter ranges. Indeed, the code is flexible enough to incorporate any form of magnetic field, even those specified by a series of data points. The next important development requires the extension to axisymmetry which will provide a clearer insight into the behaviour of a fully three-dimensional MHD flow control device. A full axisymmetric model of the nonlinear flow might also verify the presence of unidirectional flow (§3) in the vicinity of a local neutral point established for example by two current-carrying coils.

The work was undertaken at the Department of Applied Mathematics and Theoretical Physics, Cambridge University and the author is greatly indebted to Dr O. Tutty for his invaluable advice on the numerical code and to his supervisor Dr A. J. Mestel for his solid advice throughout.

REFERENCES

DENNIS, S. C. R. 1985 Compact explicit finite difference approximations to the Navier–Stokes equation. In *Ninth Intl Conf. on Numerical Methods in Fluid Dynamics* (ed. Soubbaramayer & J. P. Boujot). Lecture Notes in Physics, vol. 218, p. 23. Springer.

DENNIS, S. C. R. & HUDSON, J. D. 1979 Accurate representations of partial differential equations by finite difference schemes. *J. Inst. Math. Applics* **23**, 43–51.

DENNIS, S. C. R. & HUDSON, J. D. 1980 Further accurate representations of partial differential equations by finite difference methods. *J. Inst. Math. Applics* **26**, 369–379.

GARNIER, M. 1982 Une analyse des possibilités de contrôle des surfaces libres de métaux fondus. These de Doctorat d'Etat, INPG.

GEL'FGAT, Y., PETERSON, D. & SHCHERBININ, E. 1978*a* Velocity structure of flows in non-uniform constant magnetic fields. I. Numerical calculations. *Magnitnaya Gidrodinamika*, No. 1, 66–72, (Jan.–March).

GEL'FGAT, Y., PETERSON, D. & SHCHERBININ, E. 1978*b* Velocity structure of flows in non-uniform constant magnetic fields. II. Experimental results. *Magnitnaya Gidrodinamika*. No. 2, 23–26, (April–June).

HARTMANN, J. & LAZARUS, F. 1937 Hg-Dynamics, part II. Experimental investigations on the flow of mercury in a homogeneous magnetic field. *Kgl. Danske Videnskab. Selskab, Mat.-Fys. Medd.* **15**, No. 7.

HOLROYD, R. J. & HUNT, J. C. R. 1978 Theoretical and experimental studies of liquid metal flow in strong non-uniform magnetic fields in ducts with complex geometry. In *Proc. Second Bat-Sheva Intl Seminar* (ed. H. Branover & A. Yakhot), pp. 23–43. Israel Universities Press.

KENNY, R. G. 1989 Liquid Metal flow near magnetic neutral points In *Liquid Metal Magnetohydrodynamics* (ed. J. Lielpeteris & R. Moreau), pp. 179–185. Kluwer.

KENNY, R. G. 1990 Liquid Metal flows through non-uniform magnetic fields. Ph.D. thesis, Cambridge University.

LILLICRAP, C. 1989 Liquid Metal flow control using a.c. fields. In *Liquid Metal Magneto-hydrodynamics* (ed. J. Lielpeteris & R. Moreau), pp. 363–370. Kluwer.

MURPHY, G. M. 1960 *Ordinary Differential Equations and their Solutions*. Van Nostrand.

PAI, S. 1954 Laminar flow of an electrically conducting incompressible fluid in a circular pipe. *J. Appl. Phys.* **25**, 1205–1207.

RAMOS, J. & WINOWICH, N. 1986 Magnetohydrodynamic channel flow study. *Phys. Fluids* **29**, 992–997.

REGIRER, S. A. 1960 On an exact solution of the equations of magnetohydrodynamics. *Prik. Mat. Mekh.* **24**, 383–386.

SHERCLIFF, J. A. 1965 *A Text-book of Magnetohydrodynamics*. Pergammon.

VAN DYKE, M. 1970 Entry flow in a channel. *J. Fluid Mech.* **44**, 813–823.

YUGAWA, G. & MASUDA, M. 1982 Finite element analysis of magnetohydrodynamics and its applications to Lithium blanket design of a fusion reactor. *Nuclear Engng Design* **71**, 121–136.